Energy-Efficient Vacuum Sublimation Drying of Camel Milk: Numerical Simulation and Parametric Analysis

Arshyn Altybay , Ayaulym Rakhmatulina * , Dauren Darkenbayev * , Symbat Satybaldy

Posted Date: 20 May 2025

doi: 10.20944/preprints202505.1452.v1

Keywords: heat and mass transfer; specific energy consumption; numerical simulation; thermal optimisation; Porous media; Vacuum freeze-drying; Sublimation; camel milk

 doi:10.20944/preprints202505.1452.v1

Article

Energy-Efficient Vacuum Sublimation Drying of Camel Milk: Numerical Simulation and Parametric Analysis

Arshyn Altybay [1,2,3], Ayaulym Rakhmatulina [1,*], Dauren Darkenbayev [2,*], Symbat Satybaldy [1]

[1] Department of Mechanical Engineering and Robotics, U. Joldasbekov Institute of Mechanics and Engineering, Shevchenko Str. 28, Almaty 050010, Kazakhstan
[2] Department of Computational Sciences and Statistics, Al-Farabi Kazakh National University, Almaty 050040, Kazakhstan
[3] International Engineering and Technological University, 89/21 Al-Farabi avenue, 050060 Almaty, Kazakhstan
* Correspondence: kazrah@mail.ru (A.R); dauren.kadyrovich@gmail.com (D.D.); Tel.: +7 707 558 1373 (A.R); +7 701 259 1891 (D.D.)

Abstract: This study uses both experimental and numerical investigations into the heat and mass transfer processes governing the vacuum freeze-drying of camel milk, with a specific focus on improving energy efficiency. A three-dimensional model was developed and solved using the finite element method to simulate temperature evolution and sublimation interface progression during drying. The numerical model was validated against experimental data, achieving strong agreement with an R^2 value of 0.94. A detailed parametric analysis examined the effects of shelf temperature, sample thickness, and chamber pressure on drying kinetics and energy input. Results indicate that optimising these parameters can significantly reduce energy consumption and processing time while maintaining product quality. Notably, reducing sample thickness to 4 mm shortened drying time by up to 40% and reduced specific energy consumption (SEC) from 358 to 149 kWh/kg. These findings offer valuable insights for designing more energy-efficient freeze-drying systems, with implications for sustainable milk powder production and industrial-scale process optimisation.

Keywords: heat and mass transfer; specific energy consumption; numerical simulation; thermal optimisation; Porous media; Vacuum freeze-drying; Sublimation; camel milk

1. Introduction

Camel milk is a high-quality milk with high nutritional value and health benefits. Camel milk contains a variety of nutrients such as fat, protein, vitamins, lactose, etc. [1–3]. Research has demonstrated that camel milk possesses several bioactive properties, including anti-cancer effects [4] (Magjeed, 2005), hypoallergenic characteristics [5] (Shabo et al., 2005), and anti-diabetic potential [6] (Agrawal et al., 2003).

Camel milk has recently emerged on the international dairy market, largely due to advances in powdered milk production, which offers an effective means of preserving this highly perishable product for future use. Since camel milk is often produced in remote areas, far from consumer markets, dehydration presents the most efficient option for large-scale transportation. This method also helps retain the milk's nutritional qualities. Among the available techniques, lyophilisation (freeze-drying) is considered one of the most efficient for producing milk powder.

Camel milk powder commands a premium market price of approximately €60-100 per kilogram, significantly higher than other dairy powders including cow, goat, and mare's milk products. This presents substantial economic opportunities for camel-rearing regions, particularly for countries like Kazakhstan, where camel breeding has deep cultural and historical roots. The country's vast territorial expanses provide ideal conditions for herd expansion, while existing pastoral traditions offer a strong foundation for commercial development. The combination of high market value and favourable production conditions makes camel milk powder an attractive commodity for pastoral economies with established camel farming infrastructure.

The process of transforming fresh camel milk into a powder form comes with a significant financial burden, requiring specialised tools and substantial technological investment. Vacuum sublimation

 doi:10.20944/preprints202505.1452.v1

drying has emerged as a leading technique for creating camel milk powder, demonstrating its ability to maintain both the nutritional content and desirable taste characteristics of the milk [7].

However, freeze-drying (lyophilisation) remains more energy- and time-intensive than alternative drying methods, with current industrial systems requiring 20–35 hours to produce high-quality output. This economic and operational challenge drives ongoing research to improve process efficiency-particularly in reducing energy use and production costs. Numerical simulation of heat and mass transfer during lyophilisation offers a promising pathway for optimisation, which is the focus of this study.

Substantial improvements in freeze-drying process modelling have been achieved through three decades of development in numerical simulation techniques for simultaneous heat and mass transfer [8–15].

Liapis and Litchfield (1979)[8] introduced an optimal control framework for freeze-drying, formulating the process as a time-minimisation problem with constraints on final moisture content. Their model considered radiator energy output and chamber pressure as control variables, laying the groundwork for subsequent dynamic modelling efforts. Building upon this, Liapis and Marchello (1984) [9] expanded the modelling approach to encompass both primary and secondary drying stages. Their comprehensive analysis incorporated heat and mass transfer mechanisms, providing a more detailed understanding of the freeze-drying process dynamics. Tang, Liapis, and Marchello (1986) [10] further advanced the field by developing a multi-dimensional model describing lyophilisation in vials. This model accounted for spatial variations and provided insights into the effects of vial geometry and product configuration on drying behaviour. Mascarenhas, Akay, and Pikal (1997) [11] introduced a finite element analysis approach to simulate the freeze-drying process. Their computational model enabled the prediction of temperature and moisture profiles within the product, facilitating optimisation of process parameters. Nastaj and Witkiewicz (2009) [12] focused on the mathematical modelling of primary and secondary vacuum freeze-drying stages under microwave heating. Their work highlighted the potential of microwave-assisted freeze-drying to reduce processing time while maintaining product quality. Georgiev et al. [13] (2009) addressed the computational challenges associated with large-scale simulations by implementing adaptive time-stepping methods. Their approach improved the efficiency and accuracy of simulations, particularly for complex parabolic problems encountered in freeze-drying modelling. Zhang, Zhang, and He (2010) [14] investigated the impact of a sample's porous structure on vacuum freeze-drying. Their study emphasised the significance of microstructural characteristics in influencing drying kinetics and final product quality. Scutellà et al. (2017) [15] developed a 3D mathematical model to understand atypical heat transfer observed in vial freeze-drying. Their model incorporated various heat transfer mechanisms, including conduction, convection, and radiation, providing a comprehensive tool for analysing and optimising the freeze-drying process.

Collectively, these studies have significantly contributed to the advancement of freeze-drying process modelling, offering valuable insights and tools for improving efficiency, product quality, and scalability in the pharmaceutical and food industries.

Key developments in recent research [16–21] have substantially improved our fundamental understanding of the transient heat and mass transfer mechanisms governing lyophilisation processes.

Numerical modelling of heat and mass transfer during milk freeze-drying in vials was investigated in [16], with a focus on phase transitions and mass transport. The study highlighted the critical role of heat transfer and moisture removal in determining process efficiency, offering insights for optimising dairy industry applications.

A multiphase porous media model for predicting temperature and moisture distribution during freeze-drying was developed in [17], contributing to enhanced process control. Further advancing this field, [18] combined computational simulations with experimental validation to analyse vacuum freeze-drying of delicate materials, providing practical guidance for industries processing heat-sensitive products.

We extend the scope of our earlier work [21] through three-dimensional modelling, systematic vapour pressure assessment, and detailed parametric investigations. This study investigates the heat

 doi:10.20944/preprints202505.1452.v1

and mass transfer dynamics during the vacuum sublimation drying of camel milk, employing numerical simulations and experimental validation. Gaining a comprehensive grasp of these underlying principles is crucial for refining the drying procedure, maximising its effectiveness, and guaranteeing the superior quality of the final product. Using computational models, our research seeks to uncover the intricate relationships between heat transfer, mass movement, and material characteristics as they occur during the drying phase.

Despite its advantages in preserving nutritional quality, vacuum freeze-drying is widely recognised as one of the most energy-intensive food processing methods, with specific energy consumption often exceeding that of conventional drying techniques. This poses challenges in terms of environmental impact and economic feasibility, especially in large-scale production. Therefore, optimising freeze-drying conditions to minimise energy input while maintaining product quality is essential. This study aims to contribute toward energy-efficient process design by systematically analysing the influence of drying parameters on both drying performance and energy consumption.

2. Materials and Methods

In this section, we experimentally investigate the freeze-drying process of camel milk and present a numerical method supported by a modeling tool and governing equations. To validate the proposed model, numerical results are compared with experimental data.

2.1. Experimental Study

Experiments were performed using a shelf-type vacuum freeze-dryer (model ZLGJ-300) as the primary apparatus, shown in Figure 1. In detail, equipment information provided in reference [27]. The sample is introduced into a drying chamber, where, at reduced temperatures and pressures, the ice present within the sample transforms directly into water vapour. This vapour is subsequently channeled through a vacuum network to a designated condensation chamber for collection.

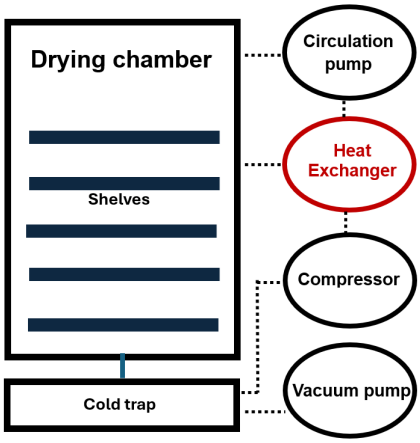

Figure 1. Schematic diagram of Experimental equipment.

Camel milk was poured into stainless steel trays $50 \times 45 \times 3$ cm at depths of 4-8 mm and placed in the freeze-drying chamber. A temperature probe was inserted into the sample to monitor core temperature. Samples were pre-frozen at $-50^{\circ}C$ for 3 hours, after which the chamber pressure was reduced to 95 Pa to initiate sublimation, with heat supplied through the shelves. Moisture loss was assessed by weighing samples every 3 hours, and moisture content was calculated from mass reduction.

Experiments were conducted using sample thicknesses of 4, 6, and 8 mm under chamber pressures of 95, 105, and 115 Pa. Preliminary trials with thicknesses greater than 8 mm showed that the final moisture content exceeded 7%, which is unacceptable by industrial standards, and the drying time was excessively long. As a result, sample thicknesses above 8 mm were excluded from this study.

 doi:10.20944/preprints202505.1452.v1

Temperature and pressure were logged every 3 minutes during drying. The complete sublimation process lasted 22–25 hours, depending on sample thickness. Drying was considered complete when the sample's weight stabilised, indicating the removal of free moisture. A visual of the dried product is shown in Figure 2.

Figure 2. Dried product.

Structural changes such as cracks, observed in Figure 2, arise from mechanical stresses due to uneven drying and shrinkage between frozen and dried layers. Although the current model assumes a rigid porous matrix, these deformations can affect heat and mass transfer by altering vapor pathways and surface exposure. Cracks may enhance mass transfer but increase heat loss, while flakes can act as thermal barriers. Future models could address these effects using a poromechanical framework.

Measurement of Moisture Content. To monitor moisture content during vacuum sublimation drying of mare's milk, we used the Evlas-2M moisture analyser, a precise instrument for analysing moisture in food and biological samples. Dried samples were collected every 3 hours, cooled to room temperature, and weighed before and after drying using a high-precision balance. Moisture content was calculated as:

$$\text{Moisture Content (\%)} = \frac{m_{\text{initial}} - m_{\text{dry}}}{m_{\text{initial}}} \times 100,$$

where. m_{initial} - is the mass of the sample before drying (wet mass), m_{dry} is the mass of the sample after complete drying (dry mass). Measurements were averaged over three trials, confirming a final moisture content below 4%, in line with industry standards. The analyzer was regularly calibrated, and results were used to validate the numerical model.

Experiment and Simulation Verification During the sublimation stage, the temperature was increased stepwise until reaching the target value. These stepwise changes were incorporated into the numerical simulation.

Figure 3 shows the comparison between simulated and experimental temperature profiles during both the primary and secondary drying stages for the 6 mm thick sample. The temperature was measured at the central part of the tray with the camel milk.

Figure 3 demonstrates a strong correlation between the numerical simulation results and the experimental temperature data. In the simulation, both cooling and heating from beneath the tray were implemented using a stepwise function.

To quantify the accuracy of the model, the coefficient of determination (R^2) was calculated using the following formula:

$$R^2 = 1 - \frac{\sum(x_i - \hat{x}_i)^2}{\sum(x_i - \bar{x})^2},$$

where x_i are the experimental temperature measurements, $\hat{x}_i$ are the simulated values, and $\bar{x}$ is the average of the experimental data. An R^2 value of 0.94 was achieved during the sublimation and drying stages, indicating excellent agreement. As illustrated in Figure 3, the model accurately reproduces the temperature evolution, confirming its reliability in capturing the heat and mass transfer dynamics of the sublimation drying process.

 doi:10.20944/preprints202505.1452.v1

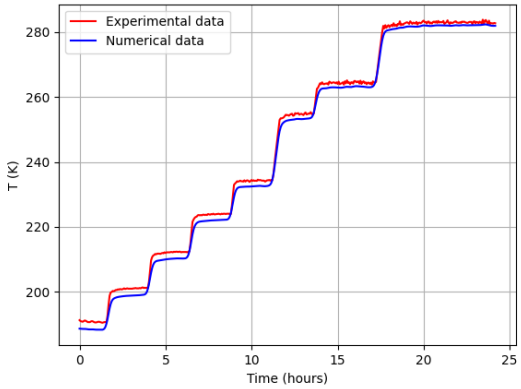

Figure 3. Comparison between the measured and simulated temperatures.

2.2. Numerical Method

Owing to the symmetry of the trays and to reduce computational time, a computational domain of $5 \times 4 \times 0.8$ cm is considered, as shown in Figure 4. The drying process divides the computational space into two regions: an uppermost, desiccated layer and a lower, frozen layer. As sublimation occurs, the boundary between these zones gradually moves downward, causing the dry area to expand. The initial drying phase ends when this sublimation front reaches the bottom of the tray.

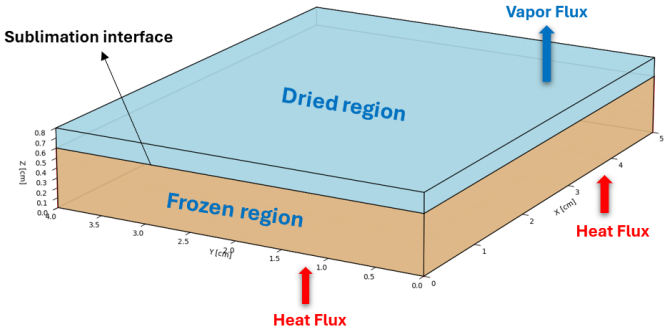

Figure 4. Computational domain

To simplify the modelling process, several assumptions were adopted based on prior studies [22]. It is assumed that the solid matrix remains structurally stable throughout the process. A thin, idealised interface separates the frozen and dried regions. Vapour transport in the dried layer is described by Darcy's law. Additionally, the porous structure is considered to remain intact as long as the temperature stays below the glass transition point.

2.2.1. Governing Equations

A computational model simulating the vacuum freeze-drying process for camel milk focuses on the interconnected nature of heat and mass movement within a porous material transforming its state. This model divides the system into two key areas: a frozen region made up of ice and the solid base material, and a dry region containing vapour and the solid base material. The transition of ice directly into vapour at their boundary causes the dry layer to expand while the frozen layer shrinks.

Heat Transfer. The temperature field $T(x, y, z, t)$ in the porous medium is governed by the energy conservation equation:

$$(\rho c_p)_{\text{eff}} \frac{\partial T}{\partial t} + \rho_v c_{p,v} \vec{u} \cdot \nabla T = \nabla \cdot (k_{\text{eff}} \nabla T) + Q_{\text{latent}}, \tag{1}$$

where $(\rho c_p)_{\text{eff}}$ is the effective volumetric heat capacity, k_{eff} is the effective thermal conductivity, $\vec{u}$ is the Darcy velocity of vapour, and Q_{latent} accounts for the latent heat absorption due to sublimation.

 doi:10.20944/preprints202505.1452.v1

Vapour Transport Vapour mass transfer u (m/s) is derived from Darcy's law, expressed as:

$$\vec{u} = -\frac{K_d}{\mu_v}\nabla p_v \tag{2}$$

where K_d is the permeability of the dried porous medium, μ_v is the dynamic viscosity of water vapour, and p_v is the vapour pressure. The relationship between vapour pressure and vapour density is maintained via the ideal gas approximation.

The corresponding water vapour pressure p_v is calculated from the vapour density ρ_v using the ideal gas law:

$$p_v = \frac{\rho_v RT}{M_v} \tag{3}$$

Here, R is the universal gas constant and M_v is the molecular weight of water vapour.

Sublimation Interface and Phase Change. The sublimation interface is tracked using a moving boundary approach based on the Clausius–Clapeyron relation:

$$T_s = \frac{\Delta H_s M_v}{R \ln\left(\frac{p_0}{p_v}\right)}, \tag{4}$$

where T_s is the sublimation temperature, ΔH_s is the latent heat of sublimation, p_0 is a reference pressure, and p_v is the vapour pressure at the interface.

The progression of the sublimation front is dictated by the principle of mass balance:

$$\rho_i \frac{dH}{dt} = -\rho_v \vec{u} \cdot \vec{n}, \tag{5}$$

where $H(t)$ is the interface position and $\vec{n}$ is the normal vector pointing outward from the frozen domain. This equation ensures that vapour flux at the interface corresponds to the rate of ice removal due to sublimation.

2.2.2. Initial and Boundary Conditions

Initially, we assume the pressure in the dehydrated area mirrors the drying chamber's pressure. Furthermore, we treat the sample as having a consistent temperature and composition throughout both the dried and frozen sections at the beginning of the sublimation drying procedure. Consequently, the starting parameters are:

$$T|_{t=0} = T_0, p|_{t=0} = p_c \tag{6}$$

3

where p_c represents the chamber pressure (in Pascals), and T_0 denotes the initial temperature (in Kelvin) of the sample material at the start of the sublimation drying process.

The mass transfer (in terms of pressure and vapour flux) boundary conditions are: At the top surface:

$$p|_{z=l_z} = p_c \tag{7}$$

At the lateral surface:

$$p|_{\omega_x} = p_c \tag{8}$$

Since water vapour is produced at the sublimation interface, the vapour flux boundary condition is established at this interface:

$$-\rho_v \frac{k_m}{\mu_v}\nabla p|_{H(t)} = \frac{\partial H(t)}{\partial t}(\rho_f - \rho_d) \tag{9}$$

where $H(t)$ represents the position of the sublimation interface. In this study, sublimation occurs in both the x- and y-directions. The heat transfer boundary conditions:

 doi:10.20944/preprints202505.1452.v1

Bottom boundary: convective heat flux from the shelf:

$$-k_{\text{eff}}\nabla T \cdot \vec{n} = h(T_s - T), \tag{10}$$

where h is the heat transfer coefficient, and T_s is the shelf temperature.

Top and lateral boundaries: convective and radiative heat losses:

$$-k_{\text{eff}}\nabla T \cdot \vec{n} = h_{amb}(T - T_{amb}) + \sigma\epsilon(T^4 - T_{amb}^4), \tag{11}$$

where h_{amb} is the ambient heat transfer coefficient, σ is the Stefan–Boltzmann constant, and ϵ is the emissivity of the surface.

The heat transfer boundary conditions in the sublimation interface:

$$T_d|_{H(t)} = T_f|_{H(t)} = T_{sub} \tag{12}$$

$$k_f \nabla T_f|_{H(t)} - k_d \nabla T_d|_{H(t)} = T_f|_{H(t)} = \frac{\partial H(t)}{\partial t}(\rho_f - \rho_d)\Delta H_s \tag{13}$$

where T_{sub} is the sublimation interface temperature (in Kelvin).

2.3. Parameters and Thermal Physical Properties

The absence of trustworthy experimental results for camel milk's thermal conductivity, density, and specific heat capacity necessitates estimations of these properties derived from the milk's established composition.

There are studies in the literature that have reported the composition of camel milk. However, slight variations in constituent content have been observed among these studies, attributed to differences in region, feeding practices, and sampling times. In this work, we adopt the results of Konuspaeva[23], as our samples originate from the same geographical area. The typical composition of camel milk is as follows in [23]: water ∼87.47%, fat ∼3.50%, protein ∼3.21%, lactose ∼4.65%, and ash: ∼0.840%. Based on the given composition of mare's milk, the following solid matrix properties have been estimated:
$k_m = 0.2997$ W/m·K (thermal conductivity), $\rho_m = 1270.6$ kg/m³ (density), $c_{p,m} = 1692.5$ J/kg·K (specific heat capacity).

To account for how thermophysical properties change across a space during sublimation, we use average properties calculated for each volume. These average properties are linked to the local ice saturation level, symbolized as S, which ranges from a state of complete freezing (S=1) to a state of complete dryness (S=0), with values in between signifying the area where sublimation is actively occurring.

The concept of effective volume-averaged density and heat capacity can be expressed effectively through the following definitions:

$$(\rho c_p)_{\text{eff}} = (1-\varepsilon)\rho_m c_{p,m} + \varepsilon\rho_I c_{p,I} + \varepsilon(1-S)\rho_v c_{p,v} \tag{14}$$

Similarly, the effective thermal conductivity, calculated using the parallel model of heat conduction in porous media, is given by:

$$k_{\text{eff}} = (1-\varepsilon)k_m + \varepsilon S k_I + \varepsilon(1-S)k_v \tag{15}$$

By setting $S = 0$, one obtains the thermophysical properties corresponding to the fully dried state of the product, as referenced in [17].

Table 1 presents a summary of the parameters employed in the numerical simulation.

Numerical simulation A three-dimensional computational model, built within the COMSOL Multiphysics 6.3 platform, was employed to simulate the freeze-drying process. This model utilized the finite element method to tackle the intricate interplay of heat and mass transfer within a porous

 doi:10.20944/preprints202505.1452.v1

structure, specifically focusing on frozen milk undergoing vacuum freeze-drying. The simulation accurately represented heat conduction and vapour movement through the frozen milk matrix by integrating the "Heat Transfer in Porous Media" and Darcy's Law modules.

Table 1. Simulation parameters for the freeze-drying procedure.

Parameter	Value	Units	Source
ε	0.705	-	[24]
ρ_m	1399.3	kg/m^3	
$c_{p,m}$	1610.7	$k \cdot J/kg \cdot K$	
k_m	0.2757	$W/m \cdot K$	
ρ_I	913	kg/m^3	[25]
$c_{p,I}$	2.090	$kJ/kg \cdot K$	[25]
k_I	2.22	$W/m \cdot K$	[25]
ρ_v	$\frac{pM_v}{RT_{dry}}$	kg/m^3	[18]
$c_{p,v}$	1.866	$kJ/kg \cdot K$	[25]
k_v	0.0022	$W/m \cdot K$	[25]
μ_v	$0.11(T/273)^{1.5}/(T+961)$	$kg/m \cdot s$	[25]
M_v	0.018	kg/mol	[17]
R	8.314	$J/mol \cdot K$	[17]
K_d	$(1-S) \times 10^{-18}(1+6.68 \times 10^5/p)$	m^2	[26]
ΔH_{sub}	2821	kJ/kg	[25]

Initially, the model presumed a completely frozen state, monitoring phase transitions through a Phase Change Interface. This feature relied on temperature-based criteria to pinpoint the boundary of sublimation. To accommodate the mesh distortion caused by volume shrinkage during ice sublimation, a Deformed Geometry component was integrated into the system. The underside experienced a defined heat input, mimicking the heat transfer from a shelf, with the sides and top edges insulated thermally. Simulations were conducted over a 24-hour period, employing a Backward Differentiation Formula (BDF) method for time progression. For improved solver reliability, a distinct method was implemented, involving two separate stages: a pressure stage and a temperature stage. Each stage utilized PARDISO, a direct linear solver, to find solutions. Nonlinear acceleration was facilitated through Anderson acceleration, employing a damping factor of 0.9, with Jacobian revisions executed at each time interval. Termination criteria for the simulation were established through bespoke formulas, designed to halt the process when the sublimation boundary reached the base of the simulated region. Thermal and material characteristics were implemented using a homogenized porous media model, incorporating newly determined values for both dry camel milk and ice.

Mesh Independence Study. For precision and dependability, a structured mesh was created using triangular elements, spanning the base of the 3D model and extending vertically. To precisely capture thermal variations, a boundary layer mesh with four enhanced layers was incorporated near regions of significant thermal influence. A globally refined mesh setting, designated as "Finer," was employed, with an even finer setting, "Extra fine," applied to critical edges. A hyperelastic smoothing technique was utilized during deformation to prevent the need for remeshing.

3. Results and Discussion

3.1. Analysis of the Movement of the Sublimation Front

A defined group of factors was chosen to model heat and mass transfer processes within camel milk during the freeze-drying procedure. This baseline encompassed a 8 mm sample depth, a shelf temperature of -20 degrees Celsius, and a reduced chamber pressure of 105 pascals.

Standard conditions reveal a clear pattern of the sublimation front's movement, as depicted in Figure 5. The grey-shaded area, symbolizing the frozen portion, steadily diminishes, retreating towards the sample's base while the dried layer grows.

 doi:10.20944/preprints202505.1452.v1

In the early stages of drying, vapour readily escapes from the top, causing the dried area to expand quickly. But as drying progresses, the growing gap between the sublimation point and the surface slows down vapour movement, thus decelerating the movement of the dried interface. Eventually, the ice crystals left at the sample's base become extremely difficult to sublimate, requiring substantial energy to eliminate completely.

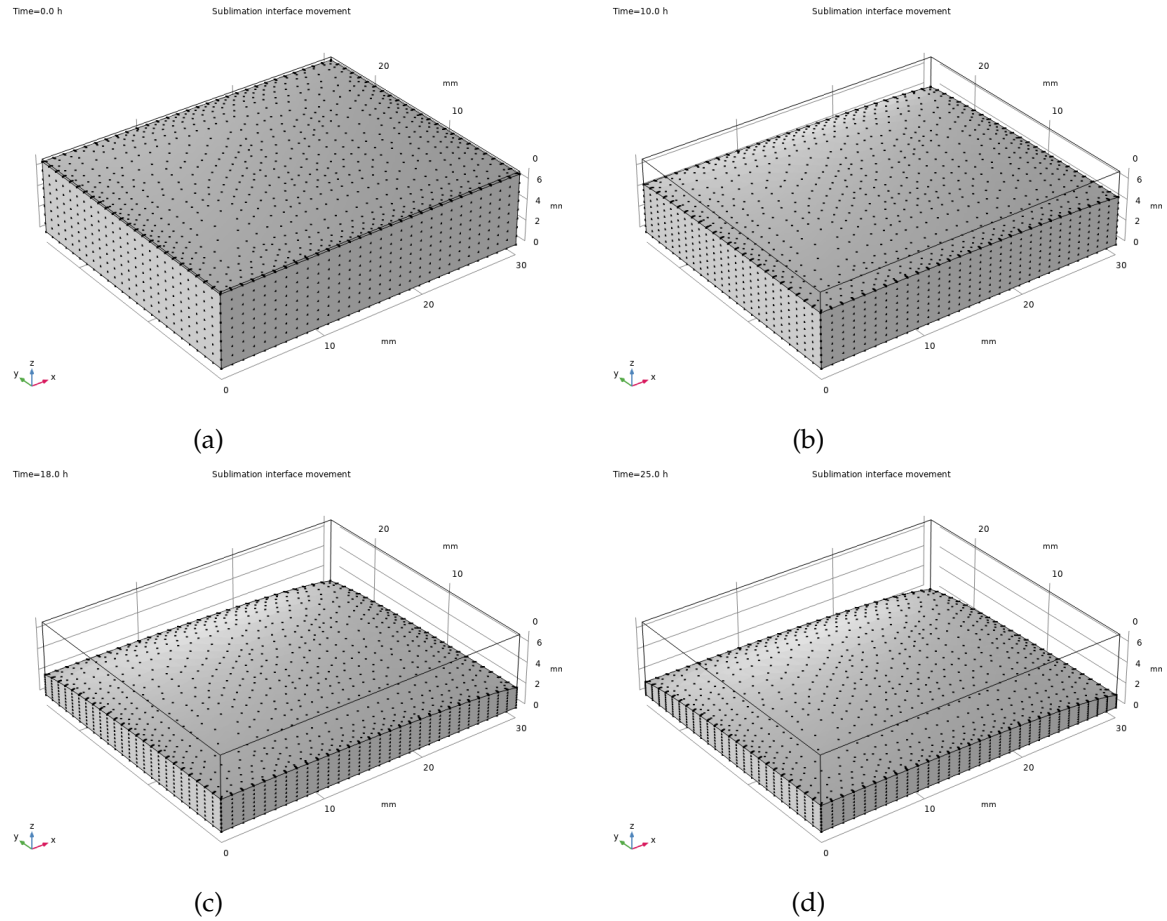

Figure 5. Progression of the sublimation interface during the drying process at the following time points: (a) 0.5 hours, (b) 5 hours, (c) 18 hours, and (d) 25 hours.

3.2. Heat and Mass Transfer Analysis

This research investigated temperature fluctuations and heat transfer patterns inside the drying chamber, revealing significant temperature differences during the initial drying stage through simulations. These disparities are a direct result of the high energy required for the transformation of ice into vapour.

Figure 6 illustrates how the temperature changes within camel milk samples during the freeze-drying process under typical circumstances. The heat emanating from the drying shelf penetrates the frozen portion of the sample, ultimately reaching the point where ice transitions directly into vapour, thus facilitating the drying.

The frozen and dried areas differ significantly in how they respond to heat. The frozen section, due to its higher thermal conductivity and ability to store heat, experiences more stable temperatures and heats up slowly. Conversely, the dry, porous layer readily absorbs radiant heat, leading to quicker, concentrated heating.

The vapour pressure patterns found in camel milk during standard freeze-drying are illustrated in Figure 7. This computational analysis, which simplifies the process by disregarding mass movement within the frozen portion, concentrates solely on how pressure changes within the dried area.

 doi:10.20944/preprints202505.1452.v1

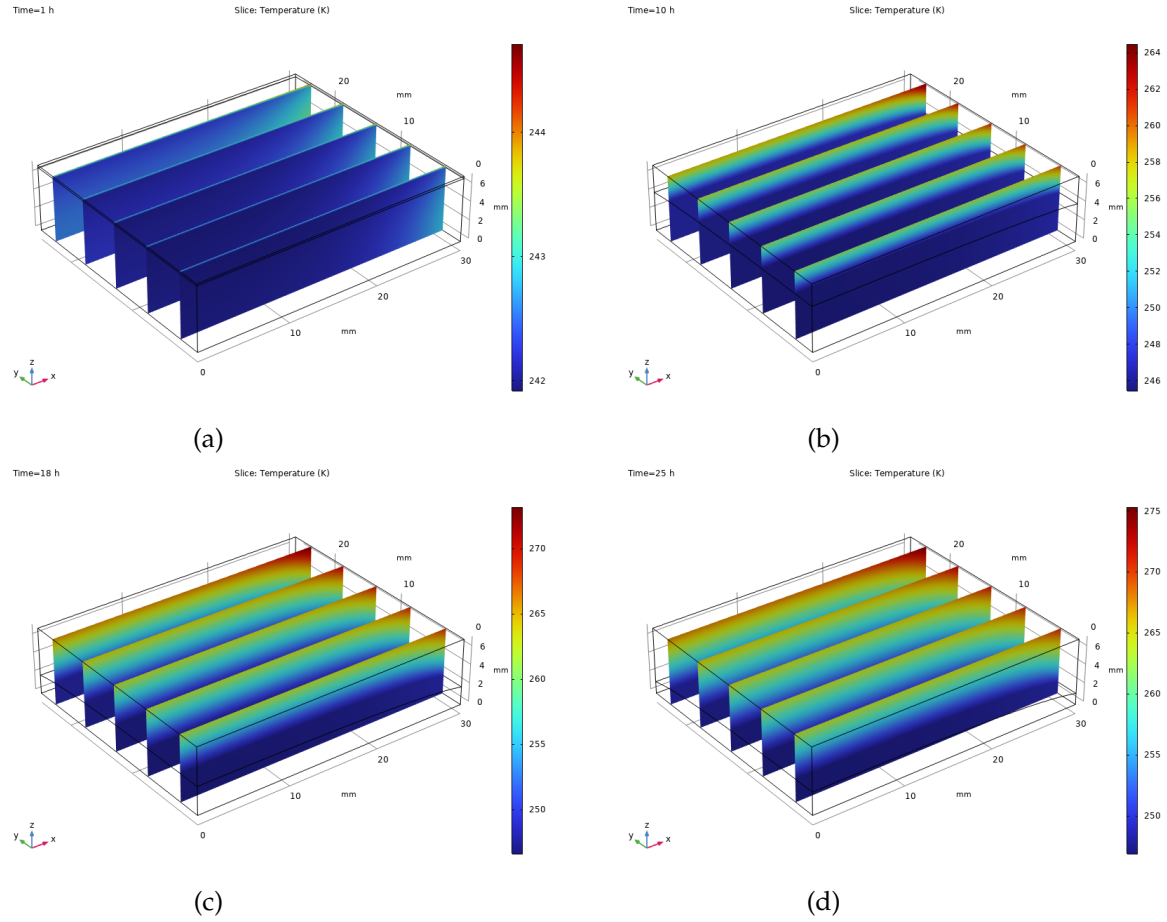

Figure 6. Heat flux distribution at different stages of the drying process.

3.3. Parametric Study

This subsection presents a comprehensive parametric analysis aimed at understanding how sample thickness and chamber pressure influence heat and mass transfer during the vacuum sublimation drying of camel milk.

We first investigated the effect of sample thickness on moisture removal efficiency. Samples with thicknesses of 4 mm, 6 mm, and 8 mm were tested under constant conditions: a shelf temperature of $-20°C$ and a chamber pressure of 105 Pa.

Figure 8a illustrates the drying duration versus moisture removal ratio for the three sample thicknesses. A clear inverse relationship is observed: thinner samples dry significantly faster. Specifically, the 4 mm sample (pink line) reaches approximately 95% moisture removal in about 10 hours, while the 6 mm sample (red line) takes roughly 15 hours, and the 8 mm sample (green line) requires nearly 20 hours to achieve 90% removal. This is attributed to shorter vapor diffusion paths in thinner samples, facilitating faster moisture escape.

Figure 8b shows the corresponding sublimation rate. Interestingly, thicker samples exhibit higher peak sublimation rates, due to the greater initial water content and stronger vapor pressure gradients. However, this advantage is offset by prolonged drying times and higher energy demand, making thinner samples more desirable from an energy efficiency perspective.

 doi:10.20944/preprints202505.1452.v1

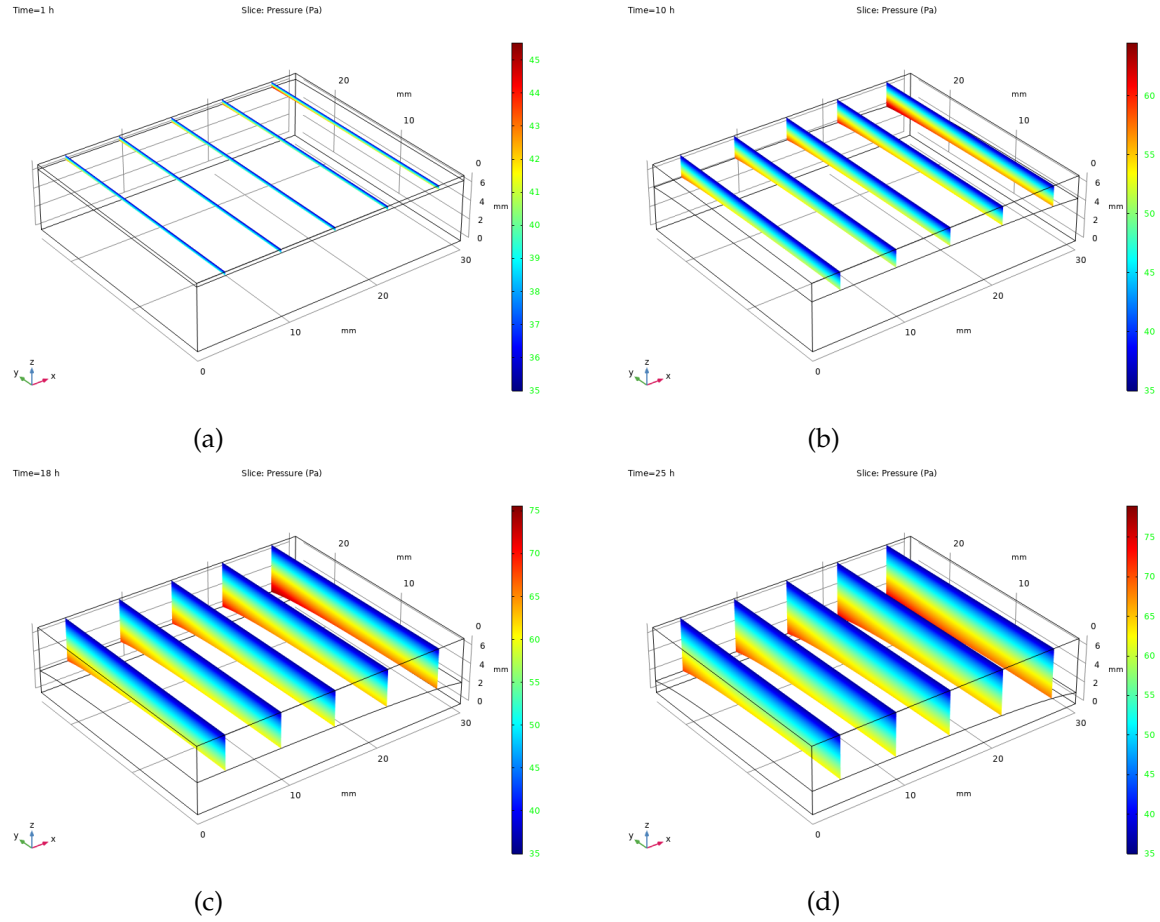

Figure 7. vapour pressure distribution throughout the sublimation drying process at different time intervals: (a) 1 hours, (b) 10 hours, (c) 18 hours, and (d) 25 hours.

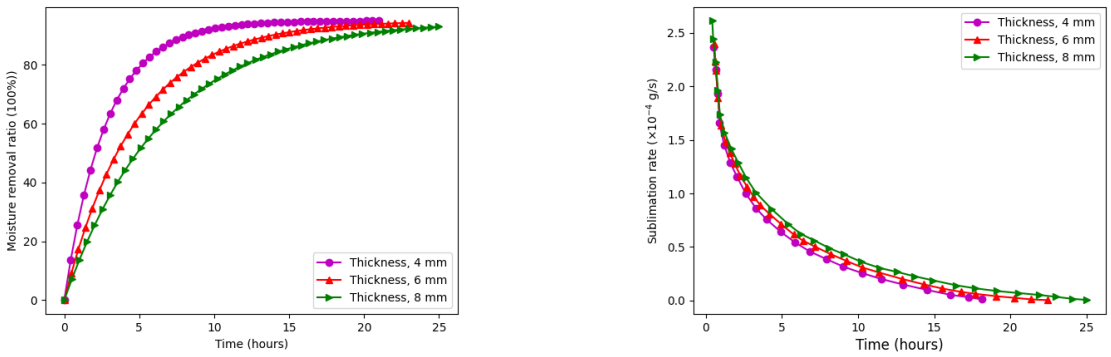

(a) **(b)**

Figure 8. Effect of sample thickness on (a) moisture removal ratio and (b) sublimation rate during the vacuum sublimation drying process.

We also studied the impact of chamber pressure on the drying process. Figure 9a shows that lowering the chamber pressure from 115 Pa to 95 Pa reduces the total drying time by approximately 30 minutes. This improvement is primarily due to enhanced vapor diffusion and a lower sublimation temperature at reduced pressure. However, it must be noted that operating the vacuum system at lower pressures incurs higher energy costs.

Figure 9b reveals that the sublimation rate initially increases with decreasing pressure, especially in the early stages. Yet, after approximately five hours, this advantage diminishes as the vapor pressure gradient stabilizes, and the sublimation rate levels off across all cases. This confirms that the benefit of pressure reduction is most significant during the early drying phase.

 doi:10.20944/preprints202505.1452.v1

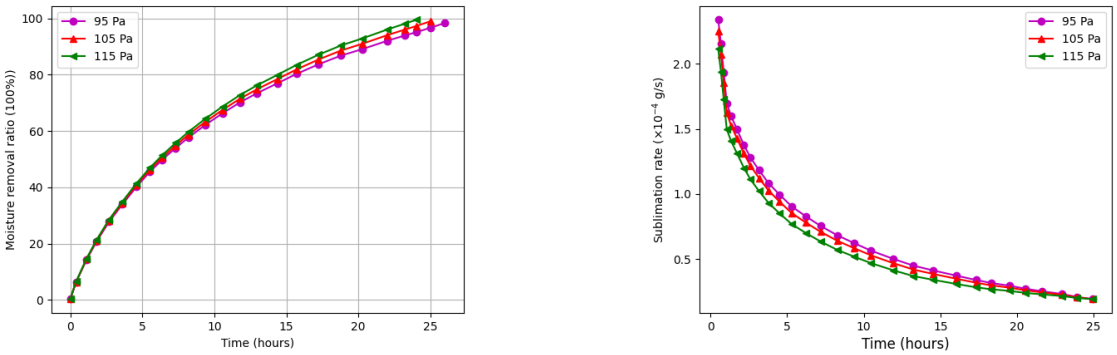

(a) **(b)**

Figure 9. Effect of chamber pressure on (a) moisture removal ratio and (b) sublimation rate.

These findings indicate that both chamber pressure and sample thickness are critical control variables for improving drying efficiency. To meet international standards requiring final moisture content below 4%, it is advisable to maintain sample thicknesses below 8 mm. Furthermore, while reduced chamber pressures accelerate drying, their contribution to energy savings must be balanced against the increased operational cost of deeper vacuum levels.

From an industrial perspective, drying performance can be scaled by using larger trays or parallel tray systems within the chamber. However, the use of very thin layers in small trays may become energetically inefficient due to the higher relative overhead. Future work will focus on integrating predictive process control, energy monitoring, and optimization algorithms to enhance sustainability and reduce the carbon footprint of freeze-drying operations in dairy processing.

3.4 Energy Performance Analysis

Evaluating energy efficiency is essential for assessing the sustainability and scalability of vacuum sublimation drying processes. In this study, we estimated the specific energy consumption (SEC) of camel milk drying based on the equipment's electrical power and the amount of water removed.

The vacuum freeze-dryer used in our experiments operates at a rated power of 14.5 kW. For typical drying durations of up to 24 hours per batch, the total energy consumed is:

$$E_{\text{total}} = 14.5\,\text{kW} \times 24\,\text{h} = 348\,\text{kWh}$$

The volume of camel milk processed in each tray was 1080 cm³ (45 cm × 40 cm × 0.6 cm), which corresponds to a mass of approximately 1.112 kg, assuming a density of 1.03 g/cm³. Given a water content of 87.47%, the mass of water removed during sublimation is:

$$m_{\text{water}} = 0.8747 \times 1.112 \approx 0.972\,\text{kg}$$

Hence, the specific energy consumption is calculated as:

$$\text{SEC} = \frac{E_{\text{total}}}{m_{\text{water}}} = \frac{348\,\text{kWh}}{0.972\,\text{kg}} \approx 358\,\text{kWh/kg}$$

To investigate how drying conditions affect energy consumption, we estimated the SEC for different sample thicknesses while keeping other parameters constant. Thinner samples dried significantly faster, reducing the total energy consumption required per unit of water removed.

Figure 10 illustrates the relationship between sample thickness and SEC. When the thickness was reduced from 8 mm to 4 mm, drying time decreased from 24 hours to 10 hours, leading to a substantial drop in SEC from 358 kWh/kg to 149 kWh/kg—a reduction of nearly 58%. This trend demonstrates that optimizing geometric and process parameters can lead to major improvements in energy performance.

 doi:10.20944/preprints202505.1452.v1

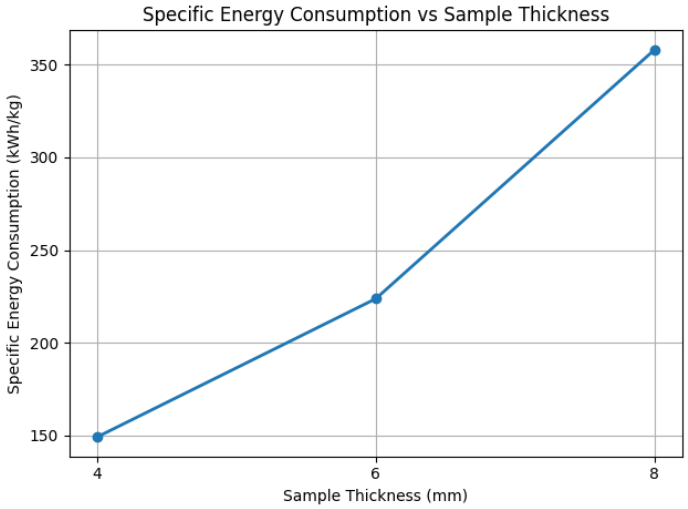

Figure 10. Specific energy consumption (SEC) versus sample thickness. Thinner samples dry faster and require less energy per unit of water removed, highlighting the importance of geometric optimisation for energy-efficient drying.

A summary of drying energy metrics across thicknesses is provided in Table 2.

Table 2. Sample thickness effect on drying time and energy consumption.

Thickness (mm)	Drying Time (h)	Energy (kWh)	SEC (kWh/kg)
4	10	145.0	149
6	15	217.5	224
8	24	348.0	358

These results emphasize that sample thickness is not only a factor in drying kinetics but also a critical determinant of energy demand. While thinner layers result in better energy performance, they may be less favorable for batch productivity. Therefore, in industrial settings, trade-offs must be considered between SEC and output volume.

Future work will involve scaling this analysis to multi-tray configurations, integrating real-time energy monitoring, and comparing SEC across various drying methods such as spray drying or microwave-assisted freeze-drying. Additionally, life-cycle energy assessment (LCEA) can be employed to quantify the environmental impact of freeze-drying and guide sustainable processing design.

4. Conclusions

This study integrated experimental measurements and three-dimensional numerical simulations to analyse the vacuum sublimation drying process of camel milk. By quantifying temperature distribution and sublimation front progression, the model demonstrated strong predictive accuracy, with an R^2 value of 0.94. Importantly, the study highlights the significant impact of process parameters such as chamber pressure and sample thickness on both drying efficiency and energy consumption.

A key contribution of this work lies in its energy-oriented analysis: reducing sample thickness and optimising chamber pressure significantly lowered drying time and improved thermal performance, thereby reducing the specific energy input per unit of removed moisture. These findings have direct implications for sustainable dairy processing and industrial freeze drying design, particularly in regions where camel milk production is expanding.

Future work will involve incorporating real-time process monitoring and control algorithms aimed at further improving energy performance, as well as conducting a comparative life cycle energy analysis with alternative drying methods. The ultimate goal is to enhance the viability of freeze-drying technology in energy constrained or sustainability-focused applications.

 doi:10.20944/preprints202505.1452.v1

Author Contributions: Conceptualization, A.A. and A.R.; methodology, A.A. and A.R.; software, D.D.; writing—review and editing, A.A and A.R.; visualisation, A.A. and S.S.; supervision, A.R.; and S.S; project administration, A.R.; funding acquisition, A.R. All authors have read and agreed to the published version of the manuscript.

Funding: This research is funded by the Committee of Science of the Ministry of Science and Higher Education of the Republic of Kazakhstan (Grant No. BR21881957).

Data Availability Statement: The original contributions presented in this study are included in the article. Further inquiries can be directed to the corresponding authors.

Conflicts of Interest: The authors declare that they have no conflicts of interest.

References

1. Konuspayeva, G.; Faye, B. Recent Advances in Camel Milk Processing. *Animals* 2021, 11, 1045. https://doi.org/10.3390/ani11041045
2. Ibrahim, A.H.; Khalifa, S.A. Effect of Freeze-Drying on Camel's Milk Nutritional Properties. *Int. Food Res. J.* **2015**, *22*, 1438–1445. https://www.proquest.com/scholarly-journals/effect-freeze-drying-on-camels-milk-nutritional/docview/1698633458/se-2.
3. Zhang, B.Y.; Xu, S.; Villalobos-Santeli, J.A.; Huang, J.-Y. Fouling Characterization of Camel Milk with Comparison to Bovine Milk. *J. Food Eng.* **2020**, *285*, 110085. https://doi.org/10.1016/j.jfoodeng.2020.110085.
4. Magjeed, N.A. Corrective Effect of Camel Milk on Some Cancer Biomarkers in Blood of Rats Intoxicated with Aflatoxin B1. *J. Saudi Chem. Soc.* **2005**, *9*, 253–263.
5. Shabo, Y.; Barzel, R.; Margoulis, M.; Yagil, R. Camel Milk for Food Allergies in Children. *Immunol. Allergy* **2005**, *7*, 796–798. https://www.scopus.com/record/display.uri?eid=2-s2.0-29444443127&origin=inward&txGid=7821cbc3977fad9e47f6be0b138afb62.
6. Agrawal, R.P.; Swami, S.C.; Beniwal, R.; Kochar, D.K.; Sahani, M.S.; Tuteja, F.C.; Ghouri, S.K. Effect of Camel Milk on Glycemic Control, Risk Factors and Diabetes Quality of Life in Type-1 Diabetes: A Randomised Prospective Controlled Study. *J. Camel Pract. Res.* **2003**, *10*, 45–50. https://www.scopus.com/inward/record.uri?eid=2-s2.0-0345770643&partnerID=40&md5=92133790c8538142a2ad8a4699fd65a7.
7. Pikal, M.J. Freeze Drying. In *Encyclopedia of Pharmaceutical Technology*; 3rd ed.; Taylor and Francis: London, UK, 2006.
8. Liapis, A.I.; Litchfield, R.J. Optimal Control of a Freeze Dryer-I: Theoretical Development and Quasi Steady State Analysis. *Chem. Eng. Sci.* **1979**, *34*, 975–981. https://doi.org/10.1016/0009-2509(79)85009-5.
9. Liapsis, A.I.; Marchello, J.M. Advances in the Modelling and Control of Freeze Drying. In *Advances in Drying*; Mujumdar, A.S., Ed.; Hemisphere Publishing Corporation: Washington, DC, USA, 1984; Volume 3, pp. 217–244.
10. Tang, M.M.; Liapis, A.I.; Marchello, J.M. A Multi-Dimensional Model Describing the Lyophilization of a Pharmaceutical Product in a Vial. In *Proc. 5th Int. Drying Symp.*; Mujumdar, A.S., Ed.; Hemisphere Publishing Corporation: New York, NY, USA, 1986; pp. 57–64.
11. Mascarenhas, W.J.; Akay, H.U.; Pikal, M.J. A Computational Model for Finite Element Analysis of the Freeze-Drying Process. *Comput. Methods Appl. Mech. Eng.* **1997**, *148*, 105–124. https://doi.org/10.1016/S0045-7825(96)00078-3.
12. Nastaj, J.F.; Witkiewicz, K. Mathematical Modeling of the Primary and Secondary Vacuum Freeze Drying of Random Solids at Microwave Heating. *Int. J. Heat Mass Transf.* **2009**, *52*, 4796–4806. https://doi.org/10.1016/j.ijheatmasstransfer.2009.06.015.
13. Georgiev, K.; Kosturski, N.; Margenov, S.; Starý, J. On Adaptive Time Stepping for Large-Scale Parabolic Problems: Computer Simulation of Heat and Mass Transfer in Vacuum Freeze-Drying. *J. Comput. Appl. Math.* **2009**, *226*, 268–274. https://doi.org/10.1016/j.cam.2008.08.020.
14. Zhang, H.; Zhang, J.; He, L. Effects of the Sample's Porous Structure on the Process of Vacuum Freeze Drying. In *IEEE Int. Conf. Bioinformatics and Biomedical Engineering* **2010**, 4244–4713. https://doi.org/10.1109/ICBBE.2010.5515695.
15. Scutella, B.; Plana-Fattori, A.; Passot, S.; Bourles, E.; Fonseca, F.; Flick, D.; Trelea, I.C. 3D Mathematical Modelling to Understand a Typical Heat Transfer Observed in Vial Freeze Drying. *Appl. Therm. Eng.* **2017**, *126*, 226–236. https://doi.org/10.1016/j.applthermaleng.2017.07.096.

 doi:10.20944/preprints202505.1452.v1

16. Srinivasan, G.; Muneeshwaran, M.; Raja, B. Numerical Investigation of Heat and Mass Transfer Behavior of Freeze Drying of Milk in Vial. *Heat Mass Transf.* **2019**, *55*, 2073–2081. https://doi.org/10.1007/s00231-018-02538-1.
17. El-Maghlany, W.M.; Bedir, A.E.; Elhelw, M.; Attia, A. Freeze-Drying Modeling via Multi-Phase Porous Media Transport Model. *Int. J. Therm. Sci.* **2019**, *135*, 509–522. https://doi.org/10.1016/j.ijthermalsci.2018.10.001.
18. Chen, B.-L.; Jang, J.-H.; Amani, M.; Yan, W.-M. Numerical and Experimental Study on the Heat and Mass Transfer of Kiwifruit during Vacuum Freeze-Drying Process. *Alex. Eng. J.* **2023**, *73*, 427–442. https://doi.org/10.1016/j.aej.2023.05.025.
19. Woo, S.-H.; Noh, J.-H.; Raza, H.; Kim, H. Numerical Modeling of Sublimation of Ammonium Carbamate Applied to Supply System of NOx Reductant. *Energies* **2021**, *14*, 3795. https://doi.org/10.3390/en14133795
20. Shao, J.; Jiao, F.; Nie, L.; Wang, Y.; Du, Y.; Liu, Z. Study on Sublimation Drying of Carrot and Simulation by Using Cellular Automata. *Processes* **2023**, *11*, 2507. https://doi.org/10.3390/pr11082507.
21. Rakhmatulina, A.; Altybay, A.; Imanbayeva, N.; Bagitova, S.; Baikonys, A. Numerical Simulation and Experimental Analysis of Mare's Milk Sublimation Drying. *Processes* **2025**, *13*, 206. https://doi.org/10.3390/pr13010206.
22. Lopez-Quiroga, E.; Antelo, L.T.; Alonso, A.A. Time-Scale Modeling and Optimal Control of Freeze–Drying. *J. Food Eng.* **2012**, *111*, 655–666. https://doi.org/10.1016/j.jfoodeng.2012.03.001.
23. Konuspayeva, G.; Faye, B.; Loiseau, G. The Composition of Camel Milk: A Meta-Analysis of the Literature Data. *J. Food Compos. Anal.* **2009**, *22*, 95–101. https://doi.org/10.1016/j.jfca.2008.09.008.
24. Song, C.S.; Nam, J.H.; Kim, C.-J.; Ro, S.T. Temperature Distribution in a Vial during Freeze-Drying of Skim Milk. *J. Food Eng.* **2005**, *67*, 467–475. https://doi.org/10.1016/j.jfoodeng.2004.04.041.
25. Nam, J.H.; Song, C.S. Numerical Simulation of Conjugate Heat and Mass Transfer during Multi-Dimensional Freeze Drying of Slab-Shaped Food Products. *Int. J. Heat Mass Transf.* **2007**, *50*, 4891–4900. https://doi.org/10.1016/j.ijheatmasstransfer.2007.08.004.
26. Warning, A.D.; Arquiza, J.M.R.; Datta, A.K. A Multiphase Porous Medium Transport Model with Distributed Sublimation Front to Simulate Vacuum Freeze Drying. *Food Bioprod. Process.* **2015**, *94*, 637–648. https://doi.org/10.1016/j.fbp.2014.08.011.
27. Experimental Setup. Available online: http://www.yuxiang17.com/productshow_161.html (accessed on 17 May 2025).